Journal of Heat and Mass Transfer Research 13 (2026), Serial Number 28, 413 – 422

Journal of Heat and Mass Transfer Research

Journal homepage: https://jhmtr.semnan.ac.ir

Semnan University

ISSN: 2383-3068

Research Article

Innovative Parametric Study on Water Extraction from Atmospheric Moisture in a Sealed Chamber via Vapor-Compression Refrigeration

Seyed Erfan Sokhangouy, Mostafa Varmazyar *

Faculty of Mechanical Engineering, Shahid Rajaee Teacher Training University, Iran

ARTICLE INFO

Article history:

Received: 2024-12-20

Revised: 2026-01-03

Accepted: 2026-01-18

Keywords:

Numerical modeling;

Humid air;

Water extraction;

Sealed chamber.

ABSTRACT

In this study, a cycle for water production from air trapped in a closed chamber is simulated and analyzed. The cycle comprises two sections: humid air and refrigerant. Humid air flows over evaporator coils, condensing water vapor into droplets. Various parameters affecting the cycle's performance, including the temperature and flow rate of incoming humid air, and the refrigerant temperature, are investigated. Through numerical modeling and parametric analysis, it is found that lower refrigerant temperatures in the evaporator significantly increase water production, especially at temperatures below 5°C. Furthermore, increasing the humid air flow rate up to 0.05 kg/s enhances dehumidification, but further increases beyond this rate reduce dehumidification as the cooling capacity is primarily used to lower air temperature. Additionally, it is observed that higher inlet air temperatures initially increase water production, with optimal flow rates varying based on temperature conditions. The ratio of latent heat to compressor power consumption improves with higher flow rates up to 0.05 kg/s, after which efficiency decreases. While the Coefficient of Performance (COP) improves with increased air flow rates, higher evaporator coil temperatures lead to reduced moisture extraction. These findings provide valuable insights for optimizing water production cycles, offering strategies to enhance efficiency for industrial and environmental applications.

1. Introduction

Water is a vital resource, playing a crucial role in the sustenance and survival of living organisms and the natural environment. Unfortunately, a significant portion of the Earth's water resources is locked in unusable forms, such as saline oceanic and sea water, or as ice in the polar regions. Given the limited availability of accessible freshwater and the critical importance of water in life, its extraction and utilization are of paramount importance. Historically, methods like drilling underground wells, creating qanats, and constructing dams have been employed to harness surface and groundwater resources. However, in recent years, the availability of these water resources has significantly diminished across various parts of the world due to increased demand driven by population growth, climate change, and the consequent reduction in precipitation, leading to widespread drought conditions. If current trends continue, the proportion of the global population facing severe water stress is projected to rise from 26.2% in 2000 to 42.4% in 2050, with an estimated 3.9 billion people experiencing severe water stress by that year [1].

* **Corresponding author.**

E-mail address: varmazyar.mostafa@sru.ac.ir

Cite this article as:

Sokhangouy, S. E. and Varmazyar, M., 2026. Innovative Parametric Study on Water Extraction from Atmospheric Moisture in a Sealed Chamber via Vapor-Compression Refrigeration. *Journal of Heat and Mass Transfer Research*, 13(4), pp. 413-422.

https://doi.org/10.22075/JHMTR.2026.36305.1662

Iran, situated within the arid and semi-arid belt of the world, is among the countries with significant water resource limitations. A review of rainfall patterns over the past five decades in Iran reveals a long-term decline, with recent years showing even further reductions in precipitation [1]. The increased exploitation of groundwater resources in recent years has inflicted irreversible damage on the country's aquifers. Overextraction has led to the intrusion of saline water into freshwater reserves across various regions of Iran. With the country's population expected to grow in the coming years, water consumption is inevitably set to increase. Given that a substantial portion of Iran's national economy is dependent on agriculture, water scarcity and drought could pose significant challenges to national and economic security. Therefore, in addition to adopting more efficient water consumption patterns, it is essential to explore alternative water sources to meet the growing demand. Technologies like seawater desalination or water production from atmospheric moisture present viable alternatives. However, seawater desalination is only feasible in regions with direct access to oceans and seas, and the high infrastructure costs for transporting water to inland areas make this process economically unviable. Furthermore, desalination plants can have various environmental impacts, including brine pollution, thermal pollution, coastal land use for plant installations, negative effects on aquifers, noise pollution, and oil spills [2-4].

Considering the limited access to seawater and the environmental challenges associated with desalination, there is a growing need to explore other sources for freshwater production. One promising alternative is harnessing atmospheric moisture. The idea of producing water from air has intrigued humanity for centuries. Observations of plants that naturally condense atmospheric moisture into dew on their leaves, or the appearance of water streaks on tree trunks during dense fogs, have fueled the concept of harvesting water from humid air. Atmospheric water extraction involves any activity that condenses and collects the water vapor present in the atmosphere [5]. This modern method of freshwater production can be particularly beneficial for people living in hot and humid regions facing water scarcity. In this method, cooling the air leads to condensation and the subsequent collection of water. Various techniques have been proposed for harvesting atmospheric moisture, including using cold deep-sea water, ground cooling, vapor-compression refrigeration cycles such as those used in air conditioners, and thermoelectric cooling systems [3, 6]. The difference between these methods lies in how the required cooling is achieved. All of these methods extract moisture from the air through cooling and can be instrumental in addressing future water shortages [7].

In recent years, there has been a significant amount of research on atmospheric water production systems. In 2018, Cattani et al. [8] conducted a detailed study on a vapor-compression refrigeration cycle with a specific evaporator and condenser arrangement for water production, evaluating its performance in terms of energy consumption under various climatic conditions for a hotel. A simulation tool was also developed to predict annual performance, energy savings, and payback periods. During testing, the device operated continuously for 24 hours, producing 1882 dm^3 of water per day, sufficient to provide 2.5 liters of water per guest per day and an additional 1724 dm^3 per day for kitchen and restaurant use. The maximum payback period was estimated at 2.5 years, based on both experimental and simulated results. In the same year, Zolfagharkhani et al. [9] conducted parametric studies on an atmospheric water generation system based on a vapor-compression refrigeration cycle. They developed a mathematical model using a precise computer algorithm to evaluate the amount of water produced and energy consumed under different environmental conditions. Their analysis considered air inlet temperatures ranging from 30 to 50°C and relative humidity from 30 to 100%. Additionally, a case study was conducted under the climatic conditions of a coastal region in Iran. The optimized small-scale model reported a water production rate of 22 to 26 liters per day with a specific energy consumption of 0.3 kWh per liter. In addition to experimental investigations, several researchers have developed numerical models for atmospheric water generation (AWG) systems in order to analyze and optimize their performance under different operating conditions. These numerical studies have consistently demonstrated that the water production rate and energy efficiency of AWG systems strongly depend on parameters such as inlet air temperature, relative humidity, air flow rate, and evaporator operating temperature. Such models provide valuable insight into the coupled heat and mass transfer processes governing dehumidification and condensation in AWG systems. For example, Raveesh et al. [10] presented a comprehensive numerical framework for simulating a vapor-compression-based AWG system, emphasizing the effects of air flow rate, ambient temperature, and humidity on system performance and water yield. Their results highlighted the critical role of evaporator temperature and operating conditions in determining both water production and energy consumption. Furthermore, a recent study [11] provides a comprehensive literature review and research gap identification on atmospheric water generation systems. In particular, Section 3 of this work presents a structured overview of existing numerical and experimental AWG models, comparing different modeling approaches, underlying assumptions, and key performance indicators.

In a related study, Eslami et al. [12] optimized a thermoelectric cooling system to achieve the best performance, considering various operational parameters to minimize energy consumption. Their parametric optimization resulted in a water production rate of 26 ml per hour at 45°C with 75% relative humidity, with an energy consumption of 20 W. In 2018, Shourideh et al. [13] designed and built a prototype atmospheric water generator using Peltier modules. Experiments were conducted under specified temperature and relative humidity conditions for two types of thermoelectric systems with different current levels and varying airflow rates. The results showed that increasing the current in the thermoelectric system led to higher water production rates but with higher specific energy consumption, thus reducing the coefficient of performance. The study also examined the effect of increasing humidity, which significantly improved the water production rate and specific energy consumption for both types of connections and all airflow rates.

More recently, researchers have explored hybrid atmospheric water harvesting (AWH) systems to improve energy efficiency [3, 14-19]. For instance, Cendoya et al. [20] evaluated a hybrid system integrating active refrigeration and vapor concentration techniques, demonstrating a 28.7% reduction in energy consumption compared to a simple vapor-compression system. Furthermore, Li et al. [21] analyzed AWH technologies from the perspective of energy trade-offs, emphasizing the need for high-volume sustainable solutions. Additionally, Cattani et al. [22] proposed a novel global evaluation index for hybrid HVAC-AWG solutions, improving efficiency assessment methodologies. A recent experimental study by Djafar et al. [23] on a vapor compression cycle-based atmospheric water generator found optimal performance at a refrigerant mass flow rate of 0.00124 kg/s and an inlet air velocity of 1.6m/s, yielding 73 ml of water per hour. This research also concluded that cooling temperatures significantly below 0°C negatively impact water production due to frost formation on the evaporator.

The main contribution of the present study is not the introduction of a new concept for atmospheric water generation (AWG), but rather the development and application of a one-dimensional transient numerical model to investigate the performance of a vapor-compression-based AWG system operating within a sealed chamber.

Unlike most existing studies, which focus on steady-state operation or open-loop systems under fixed ambient conditions, the present work analyzes the dynamic evolution of air temperature and relative humidity inside a finite-volume enclosure during the dehumidification process. Within this framework, the coupled effects of key operating parameters—such as evaporator temperature and moist air flow rate—on water production, latent heat extraction, and overall system performance are systematically examined. The results demonstrate the existence of optimal operating conditions, particularly with respect to air flow rate, beyond which water extraction performance deteriorates due to thermal limitations of the evaporator. Accordingly, this study is presented as a numerical case study intended to provide practical insights for the design and optimization of vapor-compression-based AWG systems under transient and confined operating conditions.

2. Governing Equations and Methology

In this research, the analysis of the water production system, which consists of a two-part system: a vapor-compression refrigeration cycle and a moist air cycle, has been conducted using a numerical code developed in EES software. The governing equations, including heat transfer equations for two-phase flow and pressure drop equations, are solved within this framework. The refrigerant used in the vapor-compression cycle is R134a. Initially, the refrigerant enters the compressor, where it is compressed. It then moves into the condenser, where heat exchange with the environment causes condensation. After passing through an expansion valve, the temperature and pressure of the refrigerant decrease, and it enters the evaporator as a two-phase fluid. In the moist air cycle, the moist air is directed towards the evaporator coils by a fan at a specified volumetric flow rate. Here, heat exchange occurs between the moist air and the refrigerant, causing the air temperature to drop and water droplets to form through condensation. The refrigerant, now in a superheated vapor state, exits the evaporator and re-enters the compressor. The schematic of the water production cycle is depicted in Fig. 1.

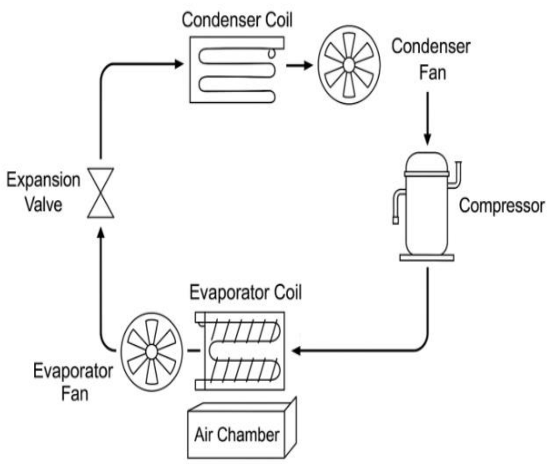

Fig. 1. Schematic of the modeled water production cycle

The compressor in the cycle has been simulated based on characteristics such as rotational speed, actual displacement, volumetric efficiency, isentropic efficiency, and effective isentropic efficiency. The volumetric efficiency determines the ratio of actual mass flow rate to the calculated mass flow rate and is used to compute the mass flow rate. The isentropic efficiency represents the ratio of the enthalpy increase during the isentropic process to the enthalpy increase under actual operating conditions. This efficiency is used to calculate the enthalpy of the fluid in the discharge line from the compressor and the power transferred to the fluid. The effective isentropic efficiency equals the ratio of the isentropic enthalpy of the fluid to the mechanical power provided. This efficiency is used to calculate the shaft power, which indicates the mechanical force required to operate the compressor. Any potential discrepancy between the shaft power and the power transferred to the fluid, due to losses such as friction, has been accounted for as heat transfer to the environment in the simulation. Other geometric characteristics of the compressor, such as the geometric volume and the relative stroke of the compressor, have also been considered in the simulation. The geometric volume indicates the calculated maximum volume of fluid compressed in each stroke. In this cycle, the inlet and outlet pressures to the compressor are 2.5 bar and 25 bar, respectively.

For simulating the condenser, an air-cooled finned tube heat exchanger has been employed. The condenser pressure is set to the compressor discharge pressure, which is 25 bar. The geometric characteristics of the condenser, including the dimensions of the heat exchanger, the geometry of the fins, the number of pipe routes in the coils, the number of coils, the material of the coils, and the wall thickness of the coils, have been specified. The two-phase condensation model has been used to simulate the refrigerant-side heat transfer in the condenser. This model addresses heat transfer during the condensation process, and the governing equations are presented in Eqs. (1) to (3). The Knackf model has been used to simulate the refrigerant pressure drop in the condenser. In this model, an initial pressure drop coefficient, which depends on the tube length, tube diameter, and flow characteristics such as velocity, density, and viscosity, is used. The pressure drop is calculated from Eq. (4).

$$\alpha = \alpha_{Liquid}((1-x)^{0.8} + \frac{3.8x^{0.76}(1-x)^{0.04}}{P_{reduced}^{0.38}}) \quad (1)$$

$$\alpha_{liquid} = 0.023Re^{0.5}pr^{0.4} \quad (2)$$

$$P_{reduced} = \frac{P}{P_{crit}} \quad (3)$$

$$dP = \zeta\frac{\rho}{2}V^2 \quad (4)$$

$$\zeta = \lambda \times \frac{L}{D} \quad (5)$$

$$\lambda = \frac{64}{Re} \qquad Re < 2300 \quad (6)$$

$$\lambda = (1.8\log(Re) - 1.5)^{-2} \; 2300 < Re < 10e^7 \quad (7)$$

In the expansion valve, significant reductions in temperature and pressure occur due to the variation in the fluid flow area. A thermostatic expansion valve is employed in the modeling. The expansion valve regulates the outlet temperature from the evaporator with the aid of a thermal bulb, ensuring that the gas exiting the evaporator is superheated to a specified degree according to the design conditions. The pressure of the gas within the thermal bulb changes based on the outlet temperature from the evaporator, and this pressure is transmitted to the diaphragm via a coiled tube. Additionally, a spring positioned at the bottom of the expansion valve, which is adjustable via a screw, allows for the creation of a specific pressure. Ultimately, the pressure differential determines the degree of opening and closing of the valve and the amount of refrigerant exiting the valve.

In the evaporator, a two-phase refrigerant interacts with the moist air flowing through the evaporator coils, leading to water condensation. For simulating this process, an MPET heat exchanger is utilized. This heat exchanger consists of plate tubes with a specified thickness, each equipped with multiple fluid inlet channels. The geometric specifications of the evaporator are detailed in Table 1. Additionally, the schematic of an MPET heat exchanger is illustrated in Fig. 2.

Table 1. Geometric specifications of the evaporator

	Description	Value
w	Width of the heat exchanger	0.2 m
h	Height of the heat exchanger	0.2 m
d	Length of the heat exchanger	0.094 m
P	Number of tube passes	2
N_t	Number of fluid inlet channels per tube	13
P_P	Diameter of each fluid inlet channel	7 mm
δ_f	Thickness of each fin	0.1 mm

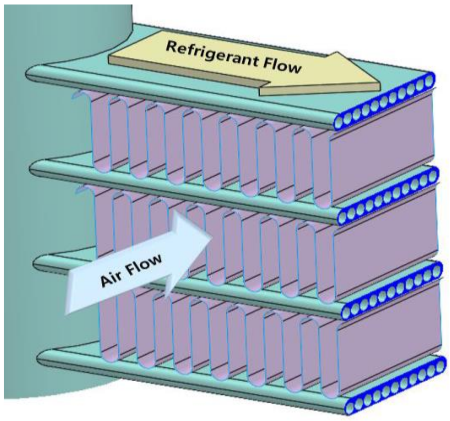

Fig. 2. Schematic of the heat exchanger [19]

The Chang-Wang heat transfer model has been employed to model the heat transfer on the air side within the evaporator. This heat transfer model is designed to calculate the heat transfer coefficient for geometries with fins and louvers, as referenced in Eq. (8) [24].

$$\alpha = \frac{j \cdot Re_{LP} \cdot Pr^{0.33}}{louverPitch \cdot \lambda} \tag{8}$$

$$Re_{LP} = \frac{Velocity \cdot louverPitch \cdot \rho}{\mu} \tag{9}$$

$$j = 0.436 Re_{LP}^{-0.559} \varepsilon^{0.192} \varepsilon_1^{0.0956} \tag{10}$$

$$\varepsilon = \frac{A}{A_t} \tag{11}$$

$$\varepsilon_1 = \frac{A_1}{A_0} \tag{12}$$

The value ε represents the fin efficiency factor. The value $\varepsilon_1$indicates the effect of the louver surface area on heat transfer. The variable A_1 denotes the louver surface area, A refers to the total area, and A_t represents the external tube surface area. The Shah-Chen two-phase heat transfer model has been utilized for the refrigerant fluid side within the evaporator. Since the Froude number compares inertial and gravitational forces, it is used to assess the impact of gravity. Therefore, the Shah method is employed for Froude numbers less than 0.04, and the Chen method is used for Froude numbers greater than 0.04 in the numerical solution. Chen proposed that the temperature gradient in the liquid near the tube wall under forced convection conditions somewhat suppresses nucleation at boiling sites, resulting in a reduced contribution of nucleate boiling. He observed that the vapor formed during the evaporation process increases the liquid velocity, thereby enhancing the contribution of convective heat transfer compared to the single-phase liquid flow [25]. Consequently, the local boiling heat transfer coefficient for two-phase flow within a tube (α_{tp}) is defined by Eq. (13).

$$\alpha_{tp} = \alpha_{FZ} S + \alpha_L F \tag{13}$$

$$\alpha_{FZ} = 0.00122 \times \left(\frac{K_L^{0.79} c_{PL}^{0.45} \rho_L^{0.49}}{\sigma^{0.5} \mu_L^{0.29} h_{LG}^{0.24} \rho_G^{0.24}} \right) \times \Delta T_{sat}^{0.24} \Delta P_{sat}^{0.75} \tag{14}$$

$$\alpha_L = 0.023 Re_L^{0.8} pr_L^{0.4} (\frac{k_L}{d_i}) \tag{15}$$

$$Re_L = \frac{\dot{m}(1-x) d_i}{\mu_L} \tag{16}$$

$$Pr_L = \frac{Cp_L \mu_L}{k_L} \tag{17}$$

$$F = (\frac{1+0.213 X_{tt}}{X_{tt}})^{0.736} \tag{18}$$

$$X_{tt} = (\frac{1-x}{x})^{0.9} (\frac{\rho_G}{\rho_L})^{0.5} (\frac{\mu_L}{\mu_G})^{0.1} \tag{19}$$

$$S = \frac{1}{1 + 0.00000253 Re_{tp}^{1.17}} \tag{20}$$

$$Re_{tp} = Re_L F^{1.25} \tag{21}$$

α_{FZ} denotes the nucleate boiling heat transfer coefficient, α_L represents the convective heat transfer coefficient of the liquid phase, ΔT_{sat} is the temperature difference between the internal tube wall (T_{wall}) and the local saturation temperature (T_{sat}), and ΔP_{sat} is the difference in vapor pressure between the wall temperature (P_{wall}) and the saturation temperature (P_{sat}). Re_L is the Reynolds number for the liquid, x is the local vapor quality, and $\dot{m}$ denotes the mass flow rate of the liquid plus vapor within the tube with an internal diameter d_i. X_{tt} is the Martinelli parameter, and Pr_L is the Prandtl number of the liquid. The two-phase multiplier F in the Chen model represents the enhancement in liquid-phase convective heat transfer due to two-phase flow, while S is the boiling suppression factor.

In the Shah method, similar to the Chen approach, two important heat transfer mechanisms—nucleate boiling and convective boiling—are considered. However, the larger value between the nucleate boiling coefficient and the convective boiling coefficient is used as the local two-phase boiling heat transfer coefficient. This method employs a dimensionless parameter N, which is referenced in Eq. (22).

$$N = 0.38Fr_L^{-0.3}C_0 \tag{22}$$

$$Fr_L = \frac{\dot{m}^2}{\rho_L^2 g d_i} \tag{23}$$

$$C_0 = \left(\frac{1-X}{X}\right)^{0.8} (\frac{\rho_G}{\rho_L})^{0.5} \tag{24}$$

$$\frac{\alpha_{cb}}{\alpha_L} = \frac{1.8}{N^{0.8}} \tag{25}$$

The effect of heat flux on nucleate boiling has been characterized using the boiling number (Bo), which represents the ratio of the actual heat flux to the maximum heat flux achievable through the complete evaporation of the fluid [25].

$$Bo = \frac{q}{\dot{m}h_{LG}} \tag{26}$$

The value of α_{nb} is calculated using one of the Eqs. (27) to (30).

$$\frac{\alpha_{nb}}{\alpha_L} = 230Bo^{0.5}, \quad Bo > 0.0003\,, N > 1 \tag{27}$$

$$\frac{\alpha_{nb}}{\alpha_L} = 1 + 46Bo^{0.5}, \quad Bo < 0.0003\,, N > 1 \tag{28}$$

$$\frac{\alpha_{nb}}{\alpha_L} = F_s Bo^{0.5}\, exp(2.74N - 0.1)\,, \quad 0.1 < N < 1 \tag{29}$$

$$\frac{\alpha_{nb}}{\alpha_L} = F_s Bo^{0.5}\, exp(2.74 - 0.15)\,, \quad N < 0.1 \tag{30}$$

In Shah's empirical correlations, the constant F_s is set to 14.7 when $Bo > 0.0011$ and 15.43 when $Bo < 0.0011$. Ultimately, the larger value between α_{nb} (nucleate boiling heat transfer coefficient) and α_{cb} (convective boiling heat transfer coefficient) is selected as α_{tp} (the two-phase boiling heat transfer coefficient). Regarding the modeling of the moist side of the evaporator, where condensation occurs, the correlations and formulations provided in Reference [26] have been employed.

The simulation is based on applying mass and energy conservation laws to various components of the system — including the evaporator, condenser, compressor, and thermal expansion valve. These components are solved iteratively until temperature convergence is achieved, ensuring an accurate and consistent solution. The transient behavior of moist air (temperature and relative humidity) in the sealed chamber is also considered in detail.

The numerical code was implemented in EES software, where the system of nonlinear equations is solved in a stepwise manner. Additionally, the built-in thermophysical property database of EES was used to obtain accurate fluid properties required for the calculations.

3. Validation and Time Step Independence

To ensure the reliability of numerical solution results, it is necessary for these results to be independent of the time step. Thus, in Table 2, the time step independence of results is examined for two primary characteristics: the refrigerant outlet temperature from the evaporator and the amount of water produced by air condensation, across several different time steps. To verify the accuracy and validity of the numerical solution, a validation is required. Figure 3 compares the numerical solution results with the experimental results from the reference study [3]. The numerical solution results from this research, shown in Fig. 3, indicate a good agreement with the experimental data in the reference article. Therefore, the numerical solution results can be considered reliable.

Table 2. Time step independence of results

Time step (s)	Amount of water produced (kg)	Refrigerant outlet temperature from the evaporator (°C)
0.4	0.0193339037	5.653995
0.2	0.0193339035	5.654659
0.1	0.0193339024	5.652728
0.05	0.0193339013	5.654059
0.025	0.0193339002	5.654025

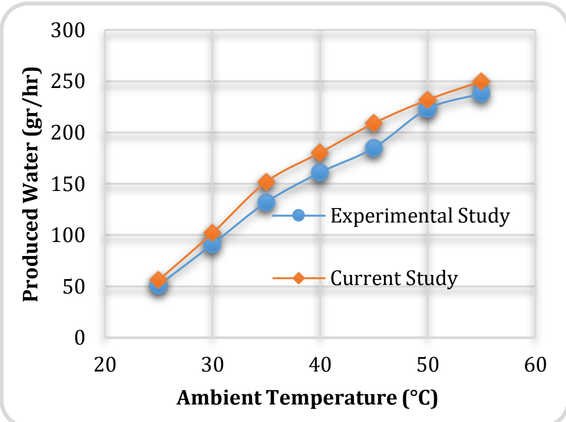

Fig. 3. Validation of numerical solution results with experimental results [3]

4. Results and Discussion

In the moisture extraction cycle from air trapped in a closed chamber, a specific volume of humid air is simulated within a fixed-volume container. The defined volume of air enters the evaporator through a fan-generated flow rate, causing condensation of the humid air. Consequently, the air exiting the evaporator loses some moisture content and re-enters the reservoir with new relative humidity conditions, mixing with the remaining air volume in the closed chamber. This mixing leads to a decrease in the humidity percentage of the new air. In subsequent phases, the air entering the evaporator will have different humidity conditions compared to the previous stage. As this cycle continues, moisture is extracted from the air within the reservoir at each stage through condensation, ultimately leading to the production of fresh water.

4.1. Effect of Refrigerant Temperature in the Evaporator on Water Production

Figure 4 illustrates the amount of water produced as a function of the refrigerant temperature in the evaporator. The water production is reported in grams per hour (g/hr), and the refrigerant temperature is indicated in degrees Celsius. The relative humidity of the incoming air over the evaporator coils is maintained constant at 43%. At evaporator temperatures below 5°C, a substantial increase in the water production rate is observed. In contrast, at evaporator temperatures above 5°C, the rate of increase in water production shows no noticeable variation.

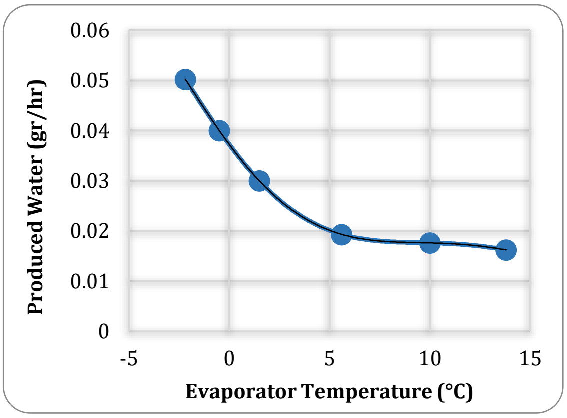

Fig. 4. Amount of water produced as a function of refrigerant temperature in the evaporator

4.2. Effect of Inlet Air Temperature on Water Production

Figure 5 illustrates the amount of water produced as a function of various inlet air flow rates to the evaporator coils at different air temperatures. As the inlet air flow rate to the evaporator coils increases, a larger volume of water vapor enters the evaporator chamber, which has the potential to produce more water. However, this increase also results in greater heat exchange between the coil and the environment, causing the coils to heat up. Consequently, as the coil temperature rises, the dehumidification process decreases. The aim is to evaluate the conditions and identify the optimal operational point for the water production system. The relative humidity of the inlet air is assumed to be constant at 43%.

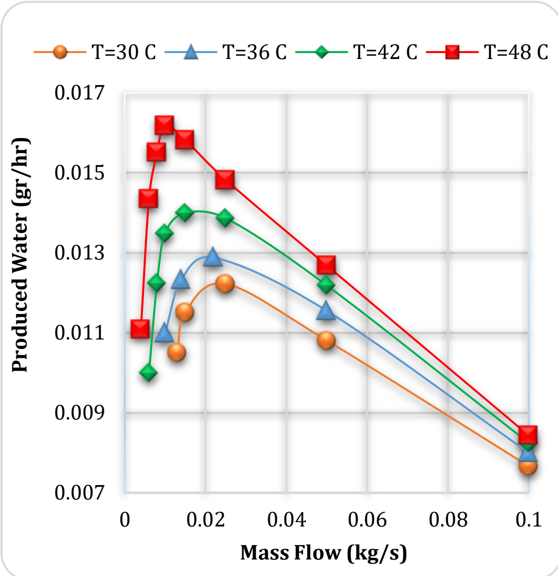

Fig. 5. Amount of water produced at different inlet air temperatures to the evaporator (60-second interval)

During a 60-second interval at temperatures of 30°C and 36°C, an initial increase in water production occurs with the rising air flow rate until it reaches a maximum at a flow rate of about 0.025 kg/s and 0.022 kg/s respectively. After this peak, further increases in flow rate lead to a decrease in water production. In contrast, at higher temperatures, like 42°C and 48°C, the conditions differ, and the maximum water production occurs at a flow rate of about 0.010 kg/s and 0.015 kg/s respectively, with subsequent increases in air flow leading to a decline in water production. At lower flow rates, the amount of water produced changes significantly with increasing air temperature.

Higher air temperatures lead to higher water production because, with constant relative humidity, the air's potential for moisture absorption increases, resulting in a larger volume of water vapor at higher temperatures. At higher flow rates, these changes diminish, making the difference in water production across various temperatures negligible at a flow rate of 0.1 kg/s.

4.3. Effect of Inlet Air Flow Rate to the Evaporator on the Amount of Latent Heat Extracted from the Cycle

Figure 6 illustrates the ratio of latent heat to the power consumption of the compressor relative to various inlet air flow rates to the evaporator coils. The cooling load extracted from the humid air passing over the coils can be divided into two components: latent heat and sensible heat. Latent heat manifests as the dehumidification of air, while sensible heat appears as a decrease in air temperature. By utilizing the ratio of latent heat to the power consumption of the compressor, one can compare the amount of moisture removal from the humid air with the energy consumption of the compressor.

Initially, as the inlet air flow rate to the evaporator coils increases up to 0.05 kg/s, the ratio of latent heat extracted from the compressor power consumption increases significantly. This increase occurs because the volume of water vapor in the air over the coils rises, leading to greater moisture extraction from the air. However, as the air flow rate exceeds 0.05 kg/s, as indicated in the graph, the ratio of latent heat to the compressor power consumption decreases, signaling a reduction in moisture extraction from the air. At higher flow rates, the compressor's energy consumption shifts from dehumidification to lowering air temperature. This phenomenon occurs because the increase in air flow rate over the coils raises the coil temperatures, consequently reducing moisture extraction efficiency.

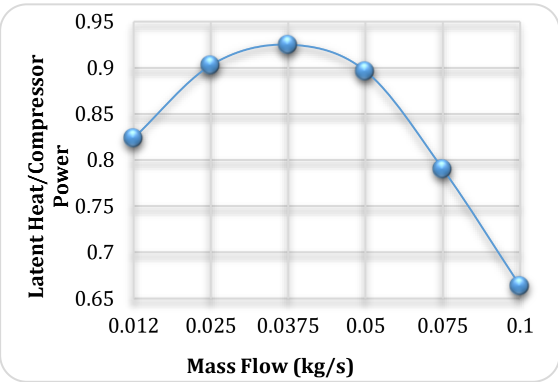

Fig. 6. Ratio of latent heat to the power consumption of the compressor relative to various inlet air flow rates to the evaporator coils

4.4. Effect of Inlet Air Flow Rate to the Evaporator on the Coefficient of Performance of the Cycle

Figure 7 shows the effect of the inlet air flow rate to the evaporator coils on the Coefficient of Performance (COP) of the cycle over a 180-second operating period. The COP is defined as the ratio of the cooling capacity of the cycle to the total power consumption, including both the compressor and fan power. As the inlet air flow rate to the coils increases, the COP of the cycle also rises, indicating that the ratio of the increase in cooling capacity to the compressor power consumption is higher. For instance, increasing the air flow rate from 0.0125 to 0.05 kg/s significantly enhances the COP.

Although the COP of the cycle improves with increasing air flow rate, the higher temperatures of the evaporator coils lead to a reduction in moisture extraction from the humid air. Consequently, a greater portion of the energy consumption is diverted from dehumidification to merely cooling the air, which is not ideal for a moisture removal cycle. Therefore, the coefficient of performance (COP) of the cycle is not acceptable within the dehumidification range, and future studies could focus on optimizing the cycle from this perspective.

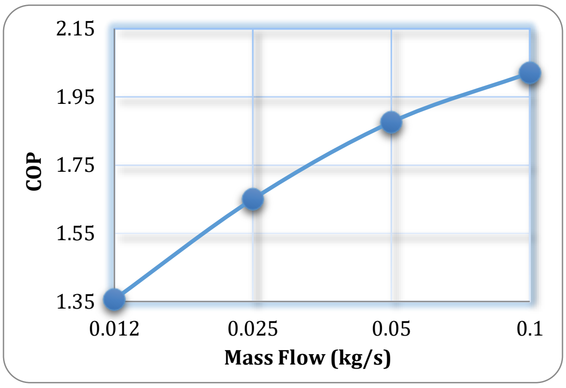

Fig. 7. Effect of inlet air flow rate to the evaporator on the Coefficient of Performance of the cycle

5. Conclusions

In this study, the performance of a water production cycle using a vapor-compression refrigeration system was investigated and analyzed. The research aimed to examine the effects of various parameters on the amount of water produced. Initially, the cycle was modeled using EES software, encompassing the refrigerant cycle and the humid air cycle, with governing equations solved numerically based on input parameters.

The results indicated that as the refrigerant temperature in the evaporator coils increased, the amount of water produced decreased. Lower temperatures resulted in higher water condensation rates, while higher temperatures were less effective for condensation.

Furthermore, the effect of inlet air temperature and flow rate on water production was analyzed. For air at temperatures of 30°C and 36°C, the amount of water produced initially increased with rising flow rates until reaching a maximum at 0.025 kg/s, after which it declined. At higher air temperatures, the peak water production occurred at 0.012 kg/s, with a decreasing trend as flow rates increased. This phenomenon was attributed to the higher moisture absorption potential of air at elevated temperatures with constant relative humidity.

The results also demonstrated that increasing the inlet air flow rate led to a decrease in the amount of water produced at constant air temperature and humidity. As flow rates increased, the coils warmed up, reducing moisture extraction efficiency. Notably, as the flow rate to the evaporator coils increased to 0.05 kg/s, the ratio of latent heat absorbed to compressor power consumption initially rose but decreased beyond this flow rate due to the compressor's energy consumption shifting to air cooling rather than moisture extraction.

Lastly, while the Coefficient of Performance (COP) of the cycle improved with increasing air flow rates, higher coil temperatures resulted in reduced moisture extraction. Consequently, more energy was consumed for cooling rather than dehumidification. Therefore, the COP of the cycle within the dehumidification range is not acceptable, and future studies should focus on optimizing the cycle from this perspective to enhance moisture extraction from humid air.

These findings provide valuable insights into the operational parameters affecting water production and system efficiency, offering a basis for future research to refine these parameters for better performance.

Nomenclature

Bo	Boiling number
c_p	Specific heat capacity at constant pressure
F_l	Fin length
F_p	Fin step
Fr_L	Froude number of liquid
h	Convection heat transfer coefficient
m_w	Mass of produced water
$\dot{m}_a$	Flow rate of moist air entering the evaporator coil
N_c	The number of cells in each path
N_t	Number of ports per coil tube
P_{shaft}	Shaft power
Pr	Prantel number
Re	Reynolds number
RH	Relative Humidity
T_a	Air temperature inside the closed chamber
T_c	The initial temperature of the condenser coils
T_e	The initial temperature of the evaporator coils
T_d	Pipe depth
T_p	Pipe pitch
x_{tt}	Martinelli parameter
α_{cb}	Convection boiling heat transfer coefficient
α_L	Heat transfer coefficient of convection boiling in the liquid phase
α_{nb}	Nuclear boiling heat transfer coefficient
α_{tp}	Boiling heat transfer coefficient for two-phase flow
δ_f	Fin thickness
ε	Fin factor
ε_1	The effect factor of the louver surface area
θ	Louvre angle
μ	Dynamic viscosity
AWG	Atmospheric Water Generation
COP	Coefficient of Performance
MHI	Moisture Harvesting Index
VCR	Vapor compression refrigeration

Funding Statement

This research did not receive any specific grant from funding agencies in the public, commercial, or not-for-profit sectors.

Conflicts of Interest

The author declares that there is no conflict of interest regarding the publication of this article.

Authors Contribution Statement

Seyed Erfan Sokhangouy: Investigation, Software, Data Curation, Formal Analysis, Visualization, Writing – Original Draft, Validation.

Mostafa Varmazyar: Supervision, Conceptualization, Methodology, Resources, Writing – Review & Editing, Project Administration.

References

[1] Mohammadjani, I., Yazdanian, N., 2013. Analysis of the water crisis situation in the country and its management requirements. *Trend Quarterly*, 21(65), pp. 117–144.

[2] Panagopoulos, A., Haralambous, K.J., 2020. Environmental impacts of desalination and brine treatment-Challenges and mitigation measures. *Marine Pollution Bulletin*, 161, p. 111773.

[3] Moradi, R., Saffarian, M.R., Behbahani-Nejad, M., 2020. Experimental study of an air humidity absorption cycle based on the MHI. *Journal of Thermal Analysis and Calorimetry*, 139(6), pp. 3613–3621.

[4] Salek, F., Moghaddam, A.N., Naserian, M.M., 2018. Thermodynamic analysis and improvement of a novel solar driven atmospheric water generator. *Energy Conversion and Management*, 161, pp. 104–111.

[5] Prada, S., da Silva, M., 2001. Fog precipitation on the Island of Madeira (Portugal). *Environmental Geology*, 41(3), pp. 384–389.

[6] Gido, B., Friedler, E., Broday, D.M., 2016. Assessment of atmospheric moisture harvesting by direct cooling. *Atmospheric Research*, 182, pp. 156–162.

[7] Wang, J., Yang, Z., Li, Z., Fu, H., Chen, J., 2025. Comprehensive review on atmospheric water harvesting technologies. *Journal of Water Process Engineering*, 69, p. 106836.

[8] Cattani, L., Magrini, A., Cattani, P., 2018. Water extraction from air by Refrigeration—Experimental results from an Integrated System Application. *Applied Sciences*, 8(11), p. 2262.

[9] Zolfagharkhani, S., Zamen, M., Shahmardan, M.M., 2018. Thermodynamic analysis and evaluation of a gas compression refrigeration cycle for fresh water production from atmospheric air. *Energy Conversion and Management*, 170, pp. 97–107.

[10] Raveesh, G., Goyal, R., Tyagi, S., 2023. Parametric analysis of atmospheric water generation system and its viability in Indian cities. *Thermal Science and Engineering Progress*, 39, p. 101682.

[11] Cattani, L., Figoni, R., Cattani, P., Magrini, A., 2025. Towards Integrated Design Tools for Water–Energy Nexus Solutions: Simulation of Advanced AWG Systems at Building Scale. *Energies*, 18(14), p. 3874.

[12] Eslami, M., Tajeddini, F., Etaati, N., 2018. Thermal analysis and optimization of a system for water harvesting from humid air using thermoelectric coolers. *Energy Conversion and Management*, 174, pp. 417–429.

[13] Shourideh, A.H., Ajram, W.B., Al Lami, J., Haggag, S., Mansouri, A., 2018. A comprehensive study of an atmospheric water generator using Peltier effect. *Thermal Science and Engineering Progress*, 6, pp. 14–26.

[14] Talib, A.J., Khalifa, A.H.N., Mohammed, A.Q., 2019. Performance study of water harvesting unit working under iraqi conditions. *International Journal of Air-Conditioning and Refrigeration*, 27(01), p. 1950011.

[15] Suranjan Salins, S., Anusha Siddiqui, S., Reddy, S.K., Kumar, S., 2021. Experimental investigation on the performance parameters of a helical coil dehumidifier test rig. *Energy Sources, Part A: Recovery, Utilization, and Environmental Effects*, 43(1), pp. 35–53.

[16] Alsheekh, M., Najim, S.E., Sultan, H.S., 2021. Air Purification and Water Generation Using A Compression Refrigeration System. *Journal of Physics: Conference Series*, 2021.

[17] Esfe, M.H., Esfandeh, S., Toghraie, D., 2021. Numerical simulation of water production from humid air for Khuzestan province: Investigation of the Peltier effect (thermoelectric cooling system) on water production rate. *Case Studies in Thermal Engineering*, 28, p. 101473.

[18] Irshad, K., Almalawi, A., Habib, K., Zahir, M.H., Ali, A., Islam, S., et al., 2021. Experimental study of a thermoelectric air duct dehumidification system for tropical climate. *Heat Transfer Engineering*, 42(13-14), pp. 1159–1171.

[19] Ullah, N., Ishaque, S., Kim, M.H., Choi, S., 2022. Modeling and Optimization of a Micro-Channel Gas Cooler for a Transcritical CO2 Mobile Air-Conditioning System. *Machines*, 10(12), p. 1177.

[20] Cendoya, A., Cuevas, C., Wagemann, E., 2023. Numerical evaluation of a hybrid atmospheric water harvesting system for human consumption. *Journal of Water Process Engineering*, 56, p. 104464.

[21] Li, H.J., Cheng, L., Sun, P., Li, F.F., Qiu, J., 2023. Potential Analysis of Atmospheric Water Harvesting Technologies from the Perspective of "Trading-in Energy for Water". *Water*, 15(5), p. 878.

[22] Cattani, L., Cattani, P., Figoni, R., Magrini, A., 2024. Performance Assessment of Atmospheric Water Generators: A Review of Evaluation Tools and Proposal for a Novel Advanced Global Evaluation Index for HVAC–AWG Hybrid Solutions. *Applied Sciences*, 14(24), p. 11793.

[23] Djafar, Z., Thufail, J.A., Nadila, S., Utamidewi, D., Mustofa, Piarah, W.H., 2025. Experimental Study: Effect of Refrigerant and Inlet Air Flow Rate on the Productivity of Atmospheric Water Generator. *International Journal of Heat and Technology*, 43(1), p. 7.

[24] Chang, Y.J., Chang, W.J., Li, M.C., Wang, C.C., 2006. An amendment of the generalized friction correlation for louver fin geometry. *International Journal of Heat and Mass Transfer*, 49(21-22), pp. 4250–4253.

[25] Thome, J., 2007. Chapter 10: Boiling heat transfer inside plain tubes, Engineering data book III. *Wolverine Tube, Inc.*

[26] Dong, J., Chen, J., Chen, Z., Zhang, W., Zhou, Y., 2007. Heat transfer and pressure drop correlations for the multi-louvered fin compact heat exchangers. *Energy Conversion and Management*, 48(5), pp. 1506–1515.